3. Using the static numerical model described above, apply a within-profile earthquake acceleration record to each node at the base of the model, and evaluate the stress and deformation behavior of the perimeter levee and geosynthetic liner system for comparison with the conventional LE/Newmark approach.

CDSM MATERIAL MODEL AND VERIFICATION

For this study, two simple embankment support numerical models incorporating CDSM *columns alone* and *columns with panels* were developed for comparison with similar, physically verified FLAC models by Filz and Navin (2006), as shown in Figures 1(a) through 1(f) below. Both the current and Filz and Navin (2006) comparison models simulated one half of an embankment (due to symmetry), with a height of 5.5 m (18 ft), half-crest width of 11 m (36 ft), and side-slope inclination of 2-to-1 horizontal to vertical (2H:1V). The simulated embankment was underlain by sand 0.6 m (2 ft) thick, lightly overconsolidated clay 8.5 m (28 ft) thick, sand 3.1 m (10 ft) thick, and a rigid base. CDSM columns were 9.8 m (32 ft) long, 0.9 m (3 ft) in diameter, and spaced 1.8 m (6 ft) center-to-center, for an area replacement ratio of 20%. CDSM panel-to-panel interface efficiency of 50% was assumed, and material types and shear strength properties used in the analysis are shown in Table 1.

Table 1 – Verification model material types and shear strength properties

Material	Total Unit Weight kN/m^3	(pcf)	Friction Angle	Cohesion kPa (ksf)
Embankment:	19.6	(125)	35°	0
Upper Sand	18.1	(115)	30°	0
Clay	15.1	(96)	0°	varies: 10.2 (0.214) top 20.6 (0.430) bottom
Lower Sand	22.0	(140)	40°	0
CDSM columns/panels	15.1	(96)	0°	689 (14.4)

To account for discontinuous CDSM columns and panels in the out-of-plane direction, composite material properties of improved ground were taken as weighted-average values based on the area replacement ratio and the shear strength properties of the CDSM material (c_{dm}) and contained soil (c_{soil}) following the approach described by Filz and Navin (2006), as follows:

$$c_{avg} = (A_R)c_{dm} + (1 - A_R)c_{soil} \qquad (1)$$

where:

c_{avg} = weighted-average cohesion of CDSM treated + untreated ground
c_{dm} = cohesion of CDSM treated ground, i.e. "soilcrete"
c_{soil} = cohesion of untreated ground
A_R = area replacement ratio = area of treated ground/area of untreated ground.

Friction angle and stiffness properties were similarly averaged, as required. As is common practice to prevent shallow failures in cohesionless embankment models, the current and comparison models applied an artificially high cohesion to the outer 2.1 m (7 ft) to 4.3 m (14 ft) of embankment material for the models with columns only and columns with panels, respectively.

Nominal stiffness properties were assigned in accordance with Filz and Navin (2006) values, and a sequential construction process was used to build the embankment, with the model allowed to equilibrate after each lift. After construction, FLAC's factor of safety solution option (FoS mode), which applies the strength reduction method (SRM, i.e., a progressive reduction in material shear strengths until the model is no longer in equilibrium), was used to evaluate the static factor of safety (FS).

Results of the model comparison are shown in Figure 1. Figures 1(c) and 1(d) show the Filz and Navin (2006) FLAC FoS mode output for columns only and columns with panels, and Figures 1(e) and 1(f) show the corresponding FLAC FoS output for the present study. The similarity of the current model results with those of the earlier study provides confidence in this study's method of simulating CDSM material behavior. The relatively minor differences between the two sets of analysis results are generally attributed to modeler-specific factors such as mesh generation, construction procedure, etc.

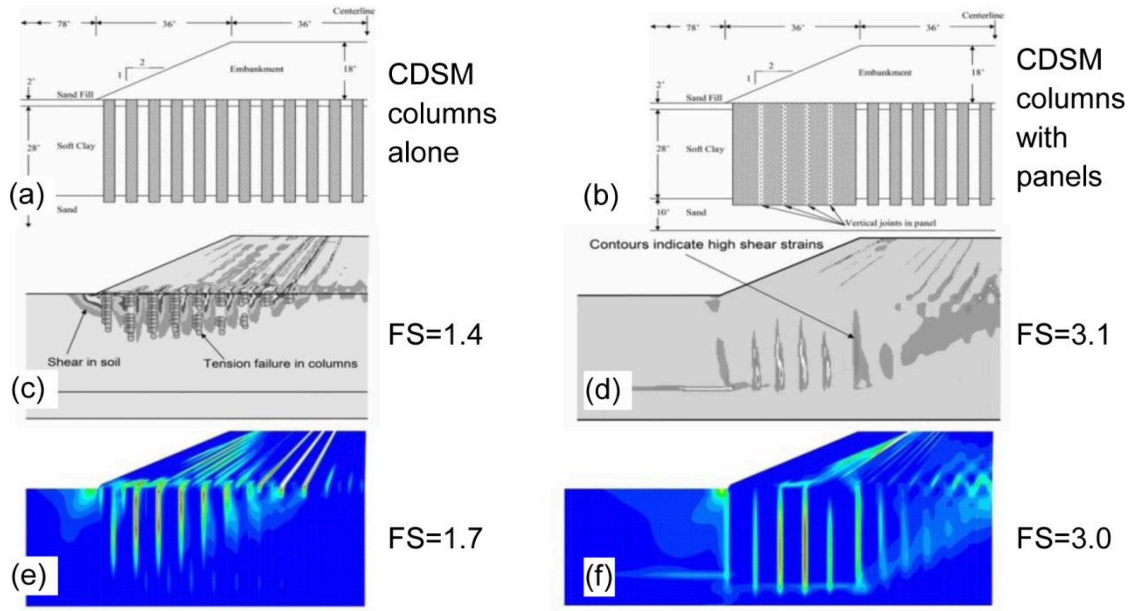

Figure 1. Geometric and FLAC model cross-sections through embankment supported by CDSM columns alone, or CDSM panels with columns; (a) to (d) Filz and Navin (2006); (e) and (f), this study.

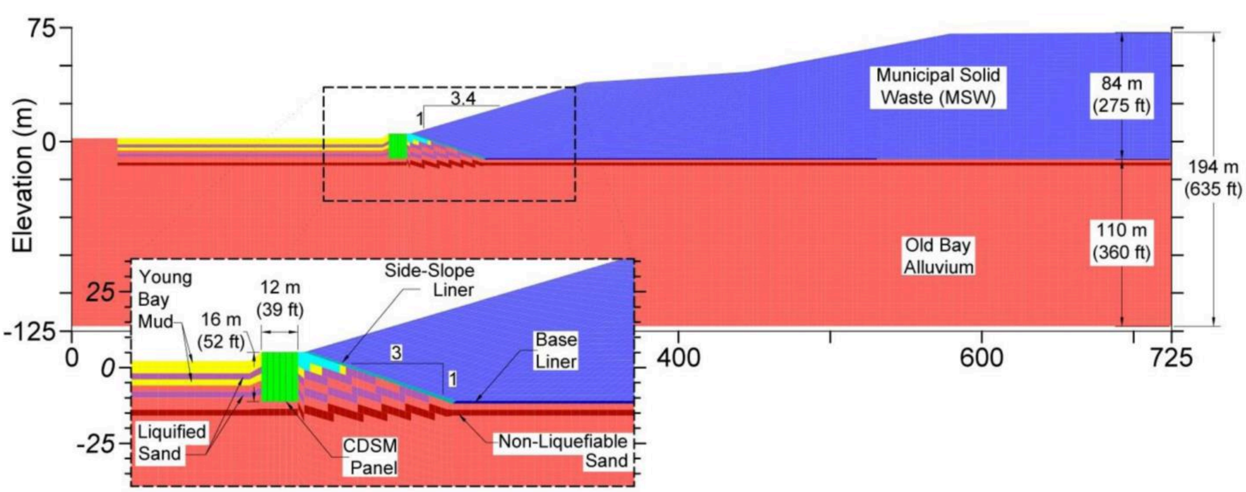

Figure 2. Newby Island Sanitary Landfill – representative cross section / FLAC model

COMPARISON WITH STATIC LIMIT EQUILIBRIUM MODEL

The NISL CDSM liquefaction mitigation design was based on a de-coupled LE pseudo-static slope stability model and Newmark-type seismic deformation analysis of a typical perimeter levee cross-section performed with the computer program SLOPE/W (Geo-Slope International, 2017). General failure modes analyzed included potential failures down through waste and along the landfill geosynthetic liner, as well as waste-subgrade failures, including some with liquefaction conditions. The development and comparison of the LE slope stability and FLAC numerical models is described below. Dimensions and material types are illustrated in Figure 2.

Limit Equilibrium-based Stability Model: Slope stability analyses were performed using Spencer's (1967) method as implemented in the computer program SLOPE/W. The model geometry and material properties were generally based on those used in the Geo-Logic Associates (2008) geotechnical report, except that final CDSM strength and layout parameters were updated to those used in the first construction phase. Ten material types were used for the slope stability model, as in Table 2.

Table 2 – Limit-equilibrium model material types and shear strength properties

Material	Total Unit Weight kN/m^3	(pcf)	Friction Angle	Cohesion kPa (ksf)
Levee fill	19.6	(125)	28°	11.5 (0.240)
Young bay mud	18.1	(115)	30°	max[0.557 x σ'$_v$, 9.6 (0.20)]
Old bay alluvium	19.6	(125)	35°	max[0.416 x σ'$_v$, 52.7 (1.10)]
Liquefied sand	19.6	(125)	0°	max[0.09 x σ'$_v$, 7.2 (0.15)]
Non-liquefied sand	19.6	(125)	32°	1.9 (.04)
CDSM panels	19.6	(125)	0°	689 (14.4)
CDSM panel-panel interfaces	19.6	(125)	0°	689 (14.4)
Side-slope liner	15.7	(100)	10°	0.2 (.004)
Base liner	15.7	(100)	14°	0.2 (.004)
Municipal solid waste	15.7	(100)	31°	43.1 (900)

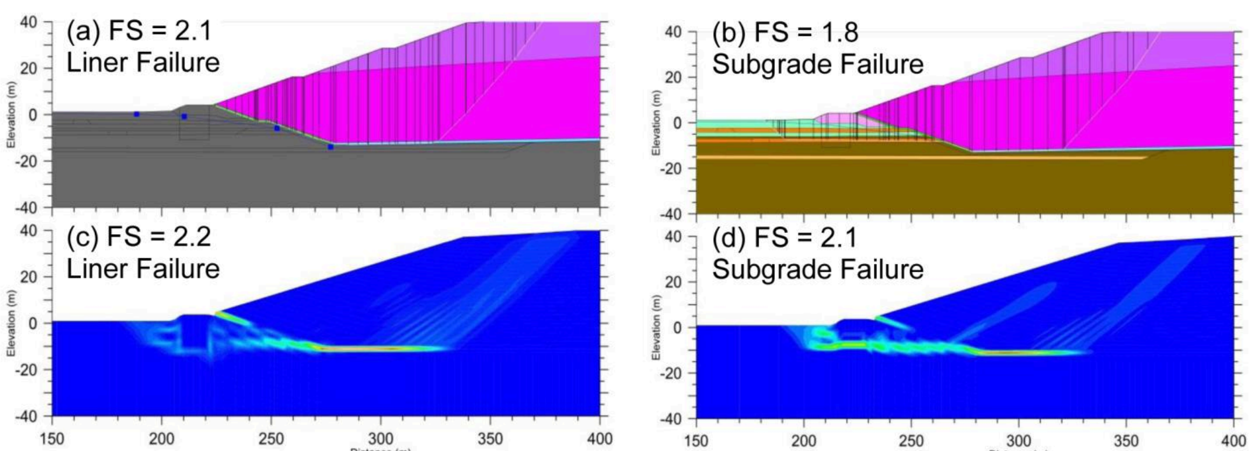

Figure 3. NISL slope stability static comparison models: (a) and (b) limit equilibrium method using SLOPE/W and (c) and (d) strength reduction method using FLAC.

Strength Reduction Method-based Numerical Stability Model: Building on the CDSM verification model discussed above, a FLAC model was developed for one NISL CDSM liquefaction mitigation design cross-section. The same ten material types were used in the FLAC model, and nominal stiffness properties were assigned to allow the model to equilibrate. Static stability analyses were performed using FLAC built-in SRM FoS mode.

For static numerical model verification, comparisons with two key LE slope stability waste fill failure modes corresponding to the controlling pre- and post-mitigation failure mechanisms were considered. A comparison of the similar post-mitigation results for LE and FLAC FoS mode methods is shown in Figure 3. In general, for both pre- and post-mitigation cases, the LE and FLAC FoS mode calculations identified the same controlling failure mechanisms (i.e., for pre-mitigation the critical failure surface aligned with the lowermost liquefiable layer; for post-mitigation the critical failure surface passing along the side-slope liner and over the perimeter levee) with reasonably similar FS values. Based on the general agreement between LE and FLAC FoS mode models, the authors have a reasonable level of confidence in the ability of the FLAC model to represent the NISL cross-section evaluated under static loading conditions.

DYNAMIC MODEL DEVELOPMENT AND PARAMETRIC STUDY

Dynamic Properties: Numerical model initial shear modulus values (G_{max}) were estimated based on a combination of site-specific soil profile shear wave velocity measurements, down to about 30 m (~100 ft), and published data for San Francisco Bay region soils (Schneider et al., 2000) and MSW (Kavazanjian et al., 2013). The following effective overburden stress (σ'_v)-based function, interpolated from the Geo-Logic Associates (2008) geotechnical report, was used to assign the initial shear modulus for all soil materials:

$$G_{max,\,soil} = -7.703\ x\ 10^{-6}\sigma'^{3}_{v} - 2.9564\ x\ 10^{-2}\sigma'^{2}_{v} + 3.8112\ x\ 10^{2}\sigma'_{v} + 4.0795\ x\ 10^{4} \qquad (2)$$

The following depth-based function, interpolated from Kavazanjian et al. (2013), and assuming a waste unit weight of 15.7 kN/m^3 (100 pcf), was used to assign G_{max} values for MSW and liner materials:

$$G_{max,MSW} = 1.8884\ x\ 10^{-2}D^{4} - 2.2645D^{3} + 72.738D^{2} + 990.53D + 32724 \qquad (3)$$

Modulus reduction and damping were incorporated in the dynamic model using FLAC's built-in hysteretic damping feature with the "default" modulus reduction curve shape. For simplicity, all materials in the model were assigned hysteretic damping function inputs corresponding to generic clay as fitted to data reported by Sun et al. (1988).

Ground Motion: The deterministic target ground motion for the NISL CDSM liquefaction mitigation design was based on the average of the Next Generation Attenuation (NGA; EERI, 2008) acceleration response spectra (ARS), with modifications to account for near-source directivity effects (Abrahamson, 2000; Somerville et al., 1997). Site response analyses were performed with SHAKE2000 (GeoMotions Suite; Matasovic and Ordonez, 2009) for multiple soil and soil/waste profiles using a suite of seven earthquake acceleration time histories (ATH) collectively scaled to the target ARS (Warner et al., 2013). Based on the average site response, the design peak horizontal ground acceleration (PHGA) for the M 7.1 maximum credible earthquake on the Hayward fault 3.3 km (2.1 miles) from the site is 0.41g. Of the seven ATHs used for site response analyses, the results with the Coronado Bridge motion (motion modified to conform the target ARS) are reported herein. This motion was applied as an SHAKE 2000 *outcrop* motion, saved as *within* motion at the base of the FLAC model, and further input as a rigid-base motion in the FLAC analysis.

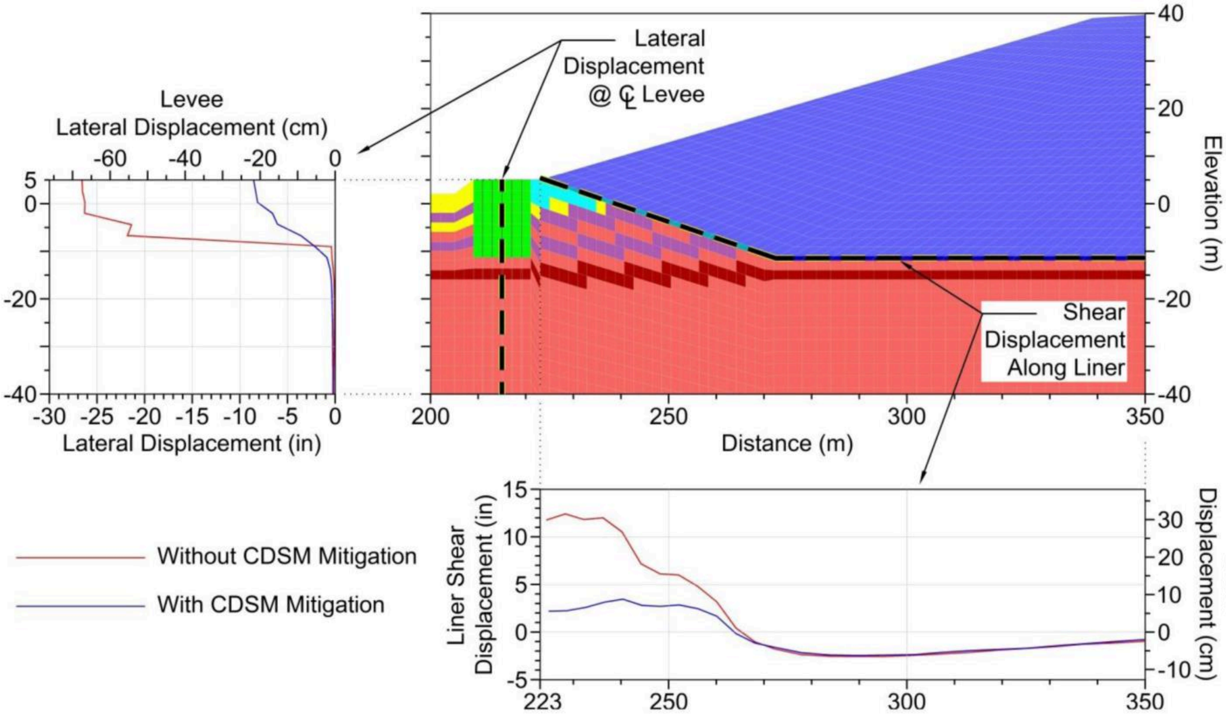

Figure 4. Model-predicted displacement parallel to the geosynthetic liner.

Dynamic Analysis Results: The representative, horizontal within-profile acceleration time history calculated using SHAKE2000, was applied along the rigid base of the FLAC model. Figure 4 shows pre- and post-mitigation model-predicted displacements at two locations: lateral displacements at the midpoint of the CDSM panels, and shear displacements along the landfill liner. As shown in the left pane of Figure 4, large lateral displacements tend to occur across the lowermost liquefiable layer without CDSM mitigation (red line). With CDSM mitigation (blue line), however, the CDSM zone intercepts this weak plane and reduces displacements significantly. The lower pane of Figure 4 shows shear displacements along the liner level, where the presence of the CDSM mitigation significantly reduces displacements (blue line) relative to the without-mitigation case (red line), particularly along the side-slope liner, where pre-mitigation shear displacements are unacceptably large relative to typical design tolerances.

Possible Design / Construction Implications: As shown in Figure 4, the CDSM program as constructed significantly reduces liquefaction-induced lateral deformation of perimeter levee and related slip along the side-slope liner to within tolerable limits. Although the focus of this study was the effect of the CDSM liquefaction mitigation on lateral displacements of the perimeter levee, it's worth noting that this mitigation has a negligible effect on slip along base liner (x > 270 m in Figure 4 lower pane). As such, additional CDSM reinforcement (e.g., larger area replacement ratio through decreased spacing and/or higher material strength) likely would not address this mechanism. Deformation of the perimeter levee contributes to slip along the side-slope liner as the levee "pulls away," and CDSM liquefaction mitigation reduces the effects of this failure mechanism. After further calibration and refinement, we expect that the FLAC dynamic numerical model developed for this study will be used to optimize the design of future NISL CDSM liquefaction mitigation phases by considering reductions in area replacement ratio, depth of treatment, and strength specifications, thereby resulting in cost savings.

SUMMARY

A CDSM liquefaction mitigation program is ongoing in support of vertical expansion of the NISL on the margins of the San Francisco Bay. Geotechnical investigations and evaluations during the design phase identified lenses of potentially liquefiable sand below the landfill perimeter levee. Design calculations showed these potentially liquefiable lenses could result in unacceptably large seismic displacements of the perimeter levee and the adjacent geosynthetically-lined landfill. A program of in-situ stabilization using CDSM elements along the levee was proposed to mitigate the potentially-excessive seismic displacements.

The design approach adopted for the CDSM program generally represents the state-of-practice for CDSM liquefaction mitigation. However, this approach does not evaluate the distribution of stresses, strains, displacements, and other parameters potentially of interest, and it does not provide a ready basis for optimization of CDSM construction specifications.

To address these limitations of the state-of-practice evaluation, a two-dimensional dynamic numerical modeling approach was developed. The landfill, CDSM-modified levee, and subsurface soils were simulated using the finite difference-based software FLAC, and design ground motions were applied at the base of the model. Preliminary numerical model results showed that the CDSM cells, as designed and constructed, will reduce perimeter levee and landfill seismic displacements to within acceptable levels. Future design phases may incorporate an optimization approach which uses two-dimensional dynamic numerical modeling to evaluate the effects of potential design modifications, including changes to CDSM unconfined compressive strength, area replacement ratio, depth of treatment, and panel-to-panel interface efficiency. It is anticipated that such an optimization approach, relative to the current state-of-practice de-coupled evaluation methodology, could result in cost savings in the design and construction of future phases of the NISL CDSM liquefaction migration program.

ACKNOWLEDGEMENTS

The authors thank Gary Lass of Geo-Logic Associates, Inc., and Anthony Luong of Republic Services, Inc., for their support and encouragement during preparation of the manuscript.

REFERENCES

Abrahamson, N.A. (2000). "Effects of rupture directivity on probabilistic seismic hazard analysis," Proc. 6th International Conference on Seismic Zonation, Palm Springs.

Filz, G.M., and Navin, M. (2006). “Stability of Column-Supported Embankments,” Report No. VTRC 06-CR13, Virginia Transportation Research Council, Charlottesville, Virginia.

Filz, G.M., Adams, T. M. , Navin, M., and Templeton, A.E. (2012). “Design of Deep Mixing for Support of Levees and Floodwalls,” Keynote Lecture, Proc. of 4th Int’l Conference on Grouting and Deep Mixing, New Orleans, LA, L.F Johnson, D.A. Bruce, M.J. Byle Eds., Geotechnical Special Publication 228, ASCE, Reston, Virginia.

Geo-Slope International (2017). “GeoStudio 2018 Software (i.e. Slope/W),” Version 9.0.4.15639, GEO-SLOPE International, Calgary, Alberta, Canada.

Geo-Logic Associates (2008). “Geotechnical Evaluation for Proposed Vertical Expansion, Newby Island Sanitary Landfill, San Jose, California,” 2 Vols., Ontario, California.

Itasca Consulting Group, Inc. (2016). “FLAC: Fast Lagrangian Analysis of Continua User’s Guide,” Version 8.00, Minneapolis, Minnesota.

Kavazanjian, E., Matasovic, N., and Bachus, R.C. (2013). “11th Peck Lecture: Predesign

Geotechnical Investigation for the OII Superfund Site Landfill," J. Geotechnical & Geoenv. Engrg., Vol. 139 (11), ASCE, Reston, Virginia, pp. 1849–1863.
Matasovic, N. and Ordonez, G.A. (2009). "GeoMotions Suite – A Suite of Computer Programs for the 1-D Analysis of Geotechnical Earthquake Engineering Problems," Quick Tutorial, GeoMotions, LLC, Lacey, Washington, 242 p.
Spencer, E. (1967). "A Method of analysis of the Stability of Embankments Assuming Parallel Inter-Slice Forces". Géotechnique.
Newmark, N.M. (1965). "Effects of earthquakes on dams and embankments," Geotechnique, Vol. 15 (2), Institution of Civil Engineers, London, 139–160.
Schneider et al. (2000). "Earthquake Scenario Ground Motion Hazard Maps for the San Francisco Bay Region," Final Technical Report, USGS Grant Award 98-HQ-GR-1004, dated May 31, 2000.
Somerville, P.G., et al. (1997). "Modification of Empirical Strong Ground Motion Attenuation Relations to Include the Amplitude and Duration Effects of Rupture Directivity," Seismological Research Letters, Vol. 68, No. 1, pp. 199.
Sun, J. I., Golesorkhi, R., and Seed, H.B. (1988). "Dynamic Moduli and Damping Ratios for Cohesive Soils," Earthquake Engineering Research Center, University of California, Berkeley, Report No. UCB/EERC-88/15, p. 42.
Warner, R.M., Lass, G.L., Pelletier, A.M, and Turk, F.J. (2013). "Investigation and Liquefaction Mitigation of Landfill Perimeter Levee," GeoCongress 2013, ASCE, Reston, Virginia.

Numerical Investigation on the Displacements and Failure Mechanism of Soil-Nailed Structures in Seismic Conditions

H. Dashtara[1]; A. H. Kolahdouzan[2]; A. Saeedi-Azizkandi[3]; and M. H. Baziar[4]

[1]M.S. Student, Dept. of Civil Engineering, Iran Univ. of Science and Technology. E-mail: hamed_dashtara@civileng.iust.ac.ir
[2]M.S. Student, Dept. of Civil Engineering, Iran Univ. of Science and Technology. E-mail: ah_kolahduzan@civileng.iust.ac.ir
[3]Assistant Professor, Dept. of Civil Engineering, Iran Univ. of Science and Technology. E-mail: asaeedia@iust.ac.ir
[4]Professor, Dept. of Civil Engineering, Iran Univ. of Science and Technology. E-mail: baziar@iust.ac.ir

ABSTRACT

A three-dimensional (3D) finite element (FE) model has been established using the commercial program ABAQUS to simulate the performance of soil nailing systems in seismic conditions. Comparisons with experimental data have confirmed that the developed FE model can simulate the seismic behavior of a soil nail system properly. Based on this, the verified FE model has been used to study the effect of different nail orientations, slope angles, and backslope angles on the seismic deformations and failure mechanism of the soil nailing systems. It was found that with an increase in nail orientation, horizontal displacement of the soil nailed system decreased almost in all of the models. However, there was an optimum value for nail inclination after which horizontal displacements started to increase or stay constant with the increase in nail inclination. As backslope angle increased, the seismic resistance of soil nailing systems became more unstable. A comparison between the results for slope angles of 75° and 90° showed that a steep nailed slope had less seismic resistance. Besides, for a slope angle of 90° the failure mechanism was a combination of translational and rotational deformations while models with slope angle equal to 75° exhibited predominantly translational failures.

INTRODUCTION

Soil nailing has been widely used as an in-situ reinforcement technique to increase the stability of slopes and deep excavations during past decades. It is a consistent and flexible system, and therefore can withstand large deformations which are induced especially during seismic events. Various post-earthquake observations (1989 Loma Prieta, 1995 Kobe, and 2001 Nisqually) have confirmed that soil nailed structures appear to show a satisfactory seismic response which has been attributed to their high flexibility (Lazarte et al. 2003). According to these observations, no major deformation or sign of distress was noticed in these structures, even though in some cases they had been subjected to horizontal acceleration as high as 0.47g (Felio et al. 1990).

Many researchers have studied the deformations and behavior of soil nailed structures. However, most of these studies are focused on static conditions and few of them have considered investigating their performance under seismic conditions. Initial studies regarding seismic behavior of soil nailing systems were performed after the 1989 Loma Prieta earthquake in San Francisco. These studies started with in-situ observations on 9 soil nailed walls and continued with dynamic centrifuge tests (Chokeir 1996).

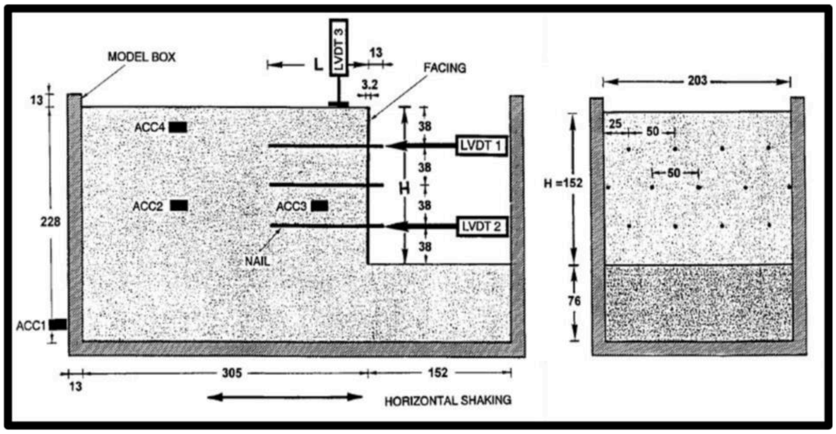

Figure1. Longitudinal and lateral cross sections of soil nailed models in dynamic centrifuge tests), All dimensions are in mm (Vucetic et al., 1993)

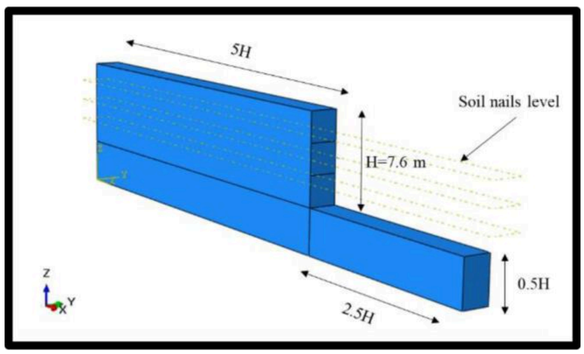

Figure2. 3D finite element model specifications

Vucetic et al. (1993) conducted a series of dynamic centrifuge tests on models of soil-nailed excavations. The models were exposed to different levels of horizontal shaking to study the seismic stability of their prototypes. In all tests, the scaling factor was 50 and the depth of the prototype excavation was H = 7.6 m. The nails in all tests were placed horizontally and their length in each test varied between 0.33H and 1H. According to the results of experiments, failure mechanism was similar in each test and occurred in two phases. First, the nails placed in bottom row acted as anchors and caused the soil-nailed mass to rotate about their connection with the facing. During the second phase, when the pullout strength of the bottom row of nails was reached due to continued strong horizontal shaking, the nailed soil mass and facing moved laterally in cyclic increments by sliding on an approximately bilinear failure surface.

Hong et al. (2005) performed a series of shaking table tests on five soil nailed steep slopes in order to investigate the effects of the angle and length of nails and the frequency amplification factor on the seismic performance and failure mechanism of the slopes. The models were 0.7 m high which represented a prototype slope with a height of 6 m. The experiments revealed that the magnitude and type of facing displacements vary with angle of soil nails. When nails were placed horizontally, the observed motion was predominantly transitional, whereas it was a combination of transition and rocking when the nails were placed with an inclination. With an increase in the length of nails, the seismic resistance of the slopes were increased. It was also noticed that an excitation with a smaller frequency amplification factor caused a greater horizontal displacement and lower seismic resistance. The failure patterns in all models were similar and could be shown with a bilinear surface.

Table1. Summary of material parameters

Material	Density	Young's modulus	Poisson's ratio	Friction angle	Cohesion	Dilation angle	α	β
Soil	1534 kg/m^3	35 MPa	0.35	36°	7.2 kPa	6°	0.00199	1.013
Nail	2000 kg/m^3	21 GPa	0.28					
Facing	2400 kg/m^3	3.1 GPa	0.35					

In this study, the finite element commercial software ABAQUS (1992) was used to assess the performance of soil nailing systems in seismic conditions. The model geometry, mesh, material constitutive models and parameters and simulation procedures are first presented. The FE model is then validated with experimental results from Vucetic et al. (1993) and comparisons between the modelling and laboratory tests are presented. Finally, the verified FE model is employed to examine the effect of different nail orientations, slope angles and backslope angles on the seismic performance and displacements of the soil nailed slopes.

FINITE ELEMENT SIMULATIONS

Geometry, mesh configuration and boundary conditions

As it was stated earlier, a three-dimensional finite element model was established using ABAQUS (1992) to simulate and analyze the seismic performance of a soil nailed systems. The geometry and instrumentation of the models in dynamic centrifuge tests conducted by Vucetic et al. (1993) and the FE numerical model are respectively shown in Figure 1 and Figure 2. Soil nailed models were 152 mm high which represent a prototype wall with a height of 7.6 m. Thus, the scaling factor in centrifuge tests equals to 50. Nails were 3.1 mm in diameter which are equivalent to prototype grouted nails with diameters of 152 mm. Furthermore, the length ratio of the soil nails was L/H = 0.76 where H is the height of the wall.

Three rows of nails were horizontally placed in the soil mass with a diamond shape pattern. The horizontal and vertical spacing of the nails were 50 mm and 38 mm respectively. The model facing was a 3.2 mm thick Plexiglas sheet representing a relatively strong and rigid prototype facing. To reduce the time of dynamic analyses, a repetitive section of the model with a diamond shape nails pattern was simulated in the numerical model.

In order to avoid the reflection of earthquake waves from the boundaries of the model, two boundaries were extended 5H and 2.5H respectively on the left and right boundaries in addition to the original length of the model. The soil mass was simulated using 8-node linear brick elements with reduced integration. Throughout the computations, an unsymmetrical matrix solver was employed because of the large deformations. Furthermore, soil nails and the facing were modeled using 2-node linear beam and 4-node doubly curved shell elements with reduced integration. Soil nails were embedded in the soil host region and the interaction between the facing and the soil were simulated using a coulomb friction model.

Pin support was applied to the bottom of the mesh so that movements in x, y and z directions